Journal of Computational and Applied Mathematics 276 (2015) 98–109

Contents lists available at ScienceDirect

Journal of Computational and Applied Mathematics

journal homepage: www.elsevier.com/locate/cam

On the numerical solution of a Stefan problem with finite extinction time

M. Vynnycky [a], S.L. Mitchell [b,*]

[a] Division of Casting of Metals, Department of Materials Science and Engineering, Royal Institute of Technology, Brinellvägen 23, 100 44 Stockholm, Sweden

[b] Mathematics Applications Consortium for Science and Industry (MACSI), Department of Mathematics and Statistics, University of Limerick, Limerick, Ireland

ARTICLE INFO

Article history:
Received 16 April 2014
Received in revised form 13 August 2014

Keywords:
Evaporation
Stefan problem
Keller box scheme
Extinction time

ABSTRACT

In many phase-change problems of practical interest, it is important to know when a phase is depleted, a quantity referred to as the extinction time; however, there are no numerical schemes that are able to compute this with any degree of rigour or formal accuracy. In this paper, we develop such a scheme for the one-dimensional time-dependent problem of an evaporating spherical droplet. The Keller box finite-difference scheme is used, in tandem with the so-called boundary immobilization method. An important component of the work is the careful use of variable transformations that must be built into the numerical algorithm in order to preserve second-order accuracy in both time and space, in particular as regards resolving a square-root singularity in the droplet radius as the extinction time is approached.

1. Introduction

The problem of the transient heating of an evaporating spherical droplet, as considered recently in [1], constitutes a phase-change (Stefan) problem that is posed on a domain initially of finite extent which vanishes after a finite time, termed hereafter as the extinction time. Whilst this situation is prevalent for evaporating drops [2], it is not the only practical situation in which this occurs: other examples are the melting or freezing of spheres [3–8], the solidification of metal in continuous casting processes [9–13], the region containing oxygen in biological tissue [14–17], and in the course of drug diffusion through polymeric spheres [18].

Whilst there exist many numerical methods for solving Stefan problems in general, there are none which are able to compute the extinction time with any level of rigour or accuracy. Indeed, whilst Mitchell et al. [1] went as far as to determine analytically that the radius of the droplet, R, would decrease with time, t, as

$$R(t) \sim (t_e - t)^{1/2}, \tag{1}$$

where t_e is the extinction time, they stopped their computations before R actually reached zero; this is also typically the case elsewhere [8,19].

Thus, the purpose of this paper is to devise a numerical scheme that is not only able to solve the Stefan problem accurately for $t < t_e$, but is also able to calculate t_e and to recover extinction behaviour of the moving boundary; in line with our recent

* Corresponding author. Tel.: +353 868952874.
E-mail addresses: sarah.mitchell@ul.ie, sarahmitc@gmail.com (S.L. Mitchell).

http://dx.doi.org/10.1016/j.cam.2014.08.023
0377-0427/

work on the use of the boundary immobilization method in tandem with the Keller box scheme for the numerical solution of Stefan problems [20–23], we once again seek to ensure that the temperature, its spatial derivative, $R(t)$ and t_e are all second-order accurate. To illustrate the idea, we will use the problem considered in [1] as an example.

The layout of this paper is as follows. In Section 2, we briefly describe the relevant equations given in [1], whereas in Section 3 we provide the auxiliary analysis that is necessary to improve the earlier numerical scheme. In Section 4, we present and discuss the new results, and conclusions are drawn in Section 5.

2. Mathematical formulation

2.1. Governing equations

A liquid fuel droplet, initially of radius R_0 and at temperature T_0, is immersed into a homogeneous hot gas at constant temperature, T_g, that is greater than T_0. Heat transfer within the droplet is assumed to occur by conduction alone; the effects of thermal radiation are ignored here, an assumption justified and discussed in more detail in [2]. At the surface of the droplet, evaporation and convection are assumed respectively to be the dominant cooling and heating mechanisms, and the radius of the droplet, $R(t)$, is expected to decrease with time t, if the effects of thermal swelling are ignored.

More details of the derivation are given in [1] but, for completeness, we summarize them now. The droplet temperature, $T(r, t)$, is governed by the heat conduction equation in spherical coordinates,

$$\rho_l c_l \frac{\partial T}{\partial t} = \frac{k_l}{r^2}\frac{\partial}{\partial r}\left(r^2 \frac{\partial T}{\partial r}\right), \quad 0 \le r < R(t),\ 0 \le t \le t_e, \tag{2}$$

where r is the distance from the centre of the droplet, c_l is the specific heat capacity of the liquid, k_l is its thermal conductivity and ρ_l its density. At this stage we introduce $\kappa = k_l/\rho_l c_l$ as the thermal diffusivity of the liquid fuel, for brevity. In addition, t_e is the time taken for the droplet to evaporate completely.

For boundary conditions, we have, at $r = 0$,

$$\frac{\partial T}{\partial r} = 0, \tag{3}$$

which expresses spherical symmetry and ensures that the temperature is bounded at $r = 0$.

At $r = R(t)$, we equate the conductive heat flux to the heat lost due to convective and evaporative cooling. This gives

$$k_l \frac{\partial T}{\partial r} + h(T - T_g) = \rho_l L \dot{R}(t), \tag{4}$$

where L is the specific heat of evaporation, and $h(t)$ is the convection heat transfer coefficient, defined by $h(t) = k_g/R(t)$, with k_g as the thermal conductivity of the gas. Note that the dot denotes differentiation with respect to t.

The moving boundary at $r = R(t)$ is controlled by fuel vapour diffusion from the droplet surface, and satisfies [24]

$$\dot{R} = -\frac{k_g \ln(1 + B_M)}{\rho_l c_g R}, \tag{5}$$

where c_g is the specific heat capacity of the gas, $B_M = \mathcal{Y}_{fs}/(1 - \mathcal{Y}_{fs})$ is the Spalding mass transfer number, and $\mathcal{Y}_{fs}$ is the mass fraction of fuel vapour near the droplet surface:

$$\mathcal{Y}_{fs} = \left[1 + \left(\frac{P_g}{P_{fs}} - 1\right)\frac{M_g}{M_f}\right]^{-1}. \tag{6}$$

Here, P_g and P_{fs} are the ambient gas pressure and the pressure of saturated fuel vapour near the surface of the droplet, respectively, and M_g and M_f are the molar masses of the gas, here assumed to be air and fuel. The variable P_{fs} is calculated from the Clasius–Clapeyron equation as

$$P_{fs} = \exp\left[a - \frac{b}{T_s - 43}\right], \tag{7}$$

where a and b are constants to be given for specific fuels and $T_s = T(R(t), t)$ is the surface temperature of the fuel droplet.

Finally, the initial conditions are

$$T(r, 0) = T_0, \qquad R(0) = R_0, \tag{8}$$

where T_0 and R_0 are constant.

We must solve the coupled equations (2) and (5) to determine $T(r, t)$ and $R(t)$, using the initial and boundary conditions specified above, noting that P_{fs} involves the unknown surface temperature T_s.

2.2. Nondimensionalization and transformation

It is more convenient to proceed in nondimensional variables. To do this, we write

$$\bar{r} = \frac{r}{R_0}, \qquad \bar{R} = \frac{R}{R_0}, \qquad \bar{t} = \frac{t}{R_0^2/\kappa}, \qquad \bar{t}_e = \frac{t_e}{R_0^2/\kappa},$$
$$\bar{T} = \frac{T - T_0}{\Delta T}, \qquad \bar{T}_g = \frac{T_g - T_0}{\Delta T}, \qquad \bar{T}_s = \frac{T_s - T_0}{\Delta T},$$

where the timescale R_0^2/κ is chosen from the heat conduction equation (2) and the temperature scale $\Delta T = L/c_l$ comes from boundary condition (4).

Upon dropping the bar notation, the governing dimensionless equations become

$$\frac{\partial T}{\partial t} = \frac{1}{r^2}\frac{\partial}{\partial r}\left(r^2\frac{\partial T}{\partial r}\right), \quad 0 \le r < R(t),\ 0 \le t \le t_e, \tag{9}$$

subject to boundary and initial conditions

$$\frac{\partial T}{\partial r} + \frac{k_{gl}\left(T - T_g\right)}{R} = \dot{R}(t) \quad \text{at } r = R(t), \tag{10}$$
$$R\dot{R} = -c_{gl}k_{gl}\ln(1 + B_M) \quad \text{at } r = R(t), \tag{11}$$
$$\frac{\partial T}{\partial r} = 0 \quad \text{at } r = 0, \tag{12}$$
$$T(r, 0) = 0, \qquad R(0) = 1, \tag{13}$$

where $k_{gl} = k_g/k_l$, $c_{gl} = c_l/c_g$. The form of (6) is unchanged, although (7) now becomes

$$P_{fs} = \exp\left[a - \frac{\beta}{T_s + \gamma}\right], \tag{14}$$

where $\beta = b/\Delta T$, $\gamma = (T_d - 43)/\Delta T$.

Finally, we make use of the standard transformation $u = rT(r, t)$ which transforms the problem into one posed on a planar geometry. Then Eqs. (9)–(13) become

$$\frac{\partial u}{\partial t} = \frac{\partial^2 u}{\partial r^2}, \quad 0 < r < R(t), \tag{15}$$

subject to the dimensionless boundary and initial conditions

$$\frac{\partial u}{\partial r} + \frac{\left(k_{gl} - 1\right)u}{R} = k_{gl}T_g + R\dot{R} \quad \text{at } r = R(t), \tag{16}$$
$$R\dot{R} = -c_{gl}k_{gl}\ln(1 + B_M) \quad \text{at } r = R(t), \tag{17}$$
$$u = 0 \quad \text{at } r = 0, \tag{18}$$
$$u(r, 0) = 0, \qquad R(0) = 1. \tag{19}$$

The forms of the expressions for B_M and $\mathcal{Y}_{fs}$ remain the same, but now

$$P_{fs} = \exp\left[a - \frac{\beta}{u_s/R + \gamma}\right], \tag{20}$$

where $u_s = u(R(t), t)$.

The numerical values of the parameters are given in Table 1.

3. Analysis

3.1. The small-time problem

An unsatisfactory feature of the numerical method in [1] was the need to switch between independent variables in order to take account of the inconsistency in $\partial u/\partial r$ between the initial condition and the boundary condition at $r = 1, t = 0$, and thereby to preserve the numerical accuracy of the scheme; recall, from [1], that a function ϕ is said to be inconsistent at $r = 1, t = 0$ if

$$\lim_{r\to 1}\phi(r, 0) \neq \lim_{t\to 0}\phi(1, t).$$

Table 1
Model parameter values, as used in [2].

Parameter	Typical value	Units
a	15.5274	–
b	5383.59	–
c_l	2400	J kg^{-1} K^{-1}
c_g	1600	J kg^{-1} K^{-1}
k_g	0.03	W m^{-1} K^{-1}
k_l	0.04	W m^{-1} K^{-1}
L	3×10^5	J kg^{-1}
M_f	0.180	kg mol^{-1}
M_g	0.029	kg mol^{-1}
P_g	3×10^6	Pa
R_0	5×10^{-6}	m
T_0	300	K
T_g	1000	K
ρ_l	700	kg m^{-3}

Here, however, we demonstrate that, by considering the small-time behaviour of the problem, we are able to construct the solution algorithm so that there is no need for a switch in variables; although this is not the main result of this paper, the issue of consistency is nevertheless a generic issue that is likely to occur in Stefan problems formulated on finite domains, which is why we include it here.

The associated small-time problem is given by

$$\frac{\partial v}{\partial t} = \frac{\partial^2 v}{\partial r^2}, \quad 0 < r < 1, \tag{21}$$

$$v = 0 \quad \text{at } r = 0, \tag{22}$$

$$\frac{\partial v}{\partial r} + c_1 v = c_2 \quad \text{at } r = 1, \tag{23}$$

$$v = 0 \quad \text{at } t = 0, \tag{24}$$

where

$$c_1 = k_{gl} - 1, \qquad c_2 = k_{gl} T_g - c_{gl} k_{gl} \ln(1 + B_{M,0}), \tag{25}$$

with $B_{M,0} = B_M(0)$. This has the solution

$$v(r, t) = \frac{c_2 r}{1 + c_1} + \sum_{n=1}^{\infty} D_n e^{-\mu_n^2 t} \sin \mu_n r, \tag{26}$$

where $(D_n)_{n=1,\ldots}$ is given by

$$D_n = \frac{2\mu_n}{\cos \mu_n \sin \mu_n - \mu_n} \int_0^1 \frac{c_2 r}{1 + c_1} \sin \mu_n r \, \mathrm{d}r, \quad n = 1, 2, \ldots \tag{27}$$

and can be simplified to

$$D_n = \frac{2c_2 \sin \mu_n}{\mu_n (\cos \mu_n \sin \mu_n - \mu_n)}, \quad n = 1, 2, \ldots$$

whereas $(\mu_n)_{n=1,\ldots}$ satisfies the transcendental equation

$$\tan \mu_n = -\frac{\mu_n}{c_1}, \quad n = 1, 2, \ldots; \tag{28}$$

from (26), note also that

$$\frac{\partial v}{\partial r}(r, t) = \frac{c_2}{1 + c_1} + \sum_{n=1}^{\infty} D_n \mu_n e^{-\mu_n^2 t} \cos \mu_n r. \tag{29}$$

Using this exact solution, it is evident that v is consistent at $(0, 0)$, since

$$\lim_{t \to 0} v(0, t) = \lim_{r \to 0} v(r, 0) = 0. \tag{30}$$

However, it is much less evident that: v is also consistent at $(1, 0)$; $\partial v/\partial r$ is consistent at $(0, 0)$; $\partial v/\partial r$ is inconsistent at $(1, 0)$. The veracity of these statements is evident in Fig. 1 where we show surface plots of v and $\partial v/\partial r$ against r and t; note the sudden change in $\partial v/\partial r$ in the vicinity of $(1, 0)$.

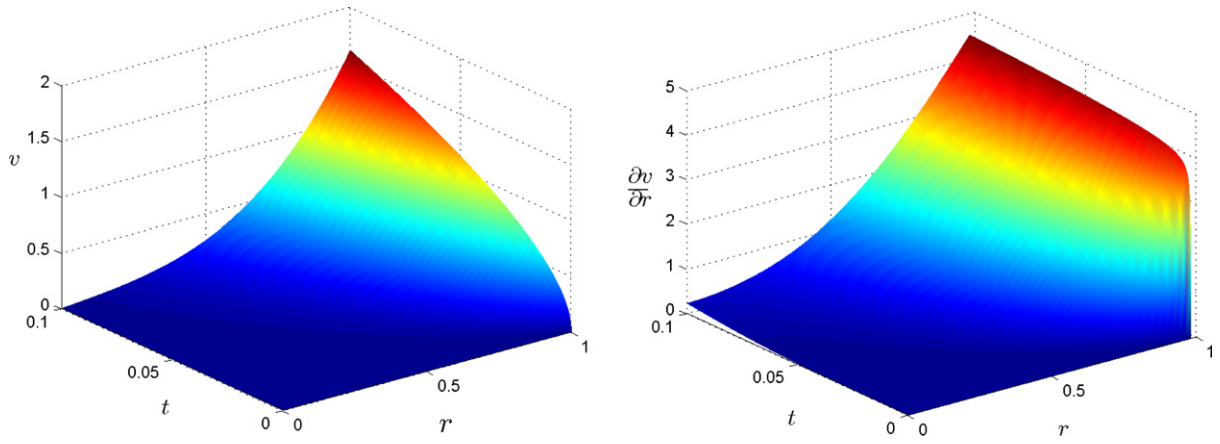

Fig. 1. Surface plots of v and $\partial v/\partial r$.

To deal with this inconsistency, we consider a problem that is related to Eqs. (21)–(24), but formulated on a semi-infinite domain, i.e.

$$\frac{\partial \hat{v}}{\partial t} = \frac{\partial^2 \hat{v}}{\partial r^2}, \quad -\infty < r < 1, \tag{31}$$

$$\hat{v} \to 0 \quad \text{at } r \to -\infty, \tag{32}$$

$$\frac{\partial \hat{v}}{\partial r} + c_1 \hat{v} = c_2 \quad \text{at } r = 1, \tag{33}$$

$$\hat{v} = 0 \quad \text{at } t = 0. \tag{34}$$

We extend the boundary at $r = 0$, as both v and $\partial v/\partial r$ are consistent at $(0, 0)$; the aim is to remove the inconsistency at $(1,\ 0)$. The problem (31)–(34) has the exact solution

$$\hat{v}(r,t) = \frac{c_2}{c_1}\,\text{erfc}\left(\frac{1-r}{2\sqrt{t}}\right) - \frac{c_2}{c_1} e^{c_1(1-r)+c_1^2 t}\,\text{erfc}\left(\frac{1-r+2c_1 t}{2\sqrt{t}}\right), \tag{35}$$

with

$$\frac{\partial \hat{v}}{\partial r}(r,t) = c_2 e^{c_1(1-r)+c_1^2 t}\,\text{erfc}\left(\frac{1-r+2c_1 t}{2\sqrt{t}}\right). \tag{36}$$

We now subtract this solution from the original problem for v, i.e. Eqs. (21)–(24), by setting

$$w(r,t) = v(r,t) - \hat{v}(r,t). \tag{37}$$

Then, the problem to solve for w becomes

$$\frac{\partial w}{\partial t} = \frac{\partial^2 w}{\partial r^2}, \quad 0 < r < 1, \tag{38}$$

$$w = -\frac{c_2}{c_1}\,\text{erfc}\left(\frac{1}{2\sqrt{t}}\right) + \frac{c_2}{c_1} e^{c_1+c_1^2 t}\,\text{erfc}\left(\frac{1+2c_1 t}{2\sqrt{t}}\right) \quad \text{at } r = 0, \tag{39}$$

$$\frac{\partial w}{\partial r} + c_1 w = 0 \quad \text{at } r = 1, \tag{40}$$

$$w = 0 \quad \text{at } t = 0. \tag{41}$$

Fig. 2 shows surface plots of w and $\partial w/\partial r$ against r and t; note that there is no discontinuity in $\partial w/\partial r$ near $(1, 0)$.

3.2. Full model equations

Let us now return to the original problem (15)–(18). We wish to subtract a function from u so that we obtain consistency for the dependent variable and its spatial derivative. We choose to subtract off $\hat{v}(r, t)$, defined in (35), and so set

$$w(r,t) = u(r,t) - \hat{v}(r,t), \tag{42}$$

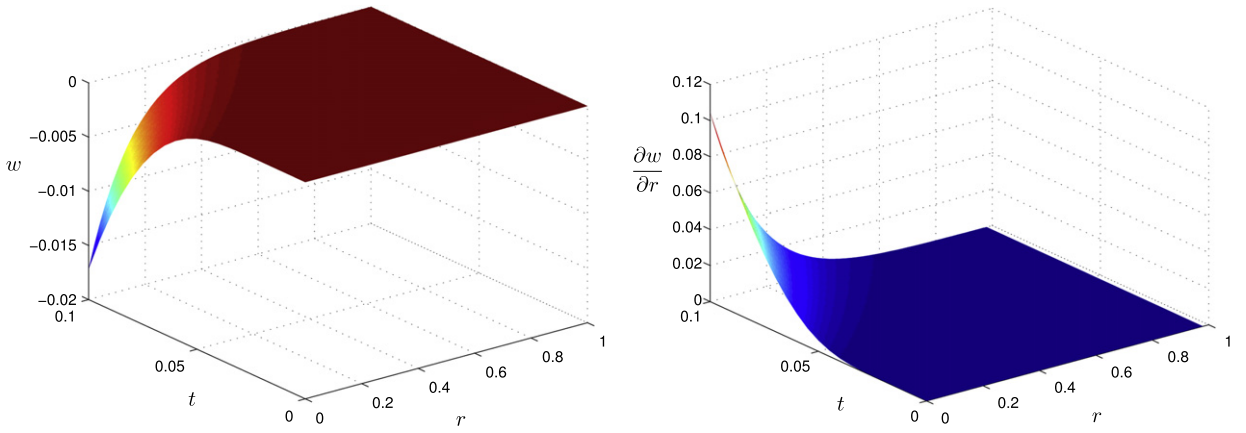

Fig. 2. Surface plots of w and $\partial w/\partial r$.

which means that the equations for w are

$$\frac{\partial w}{\partial t} = \frac{\partial^2 w}{\partial r^2}, \quad 0 < r < R,\ 0 < t < t_e \tag{43}$$

$$w = f(t) \quad \text{at } r = 0, \tag{44}$$

$$R\frac{\partial w}{\partial r} + c_1 w = g(R,t) + R^2\dot{R} \quad \text{at } r = R, \tag{45}$$

$$R\dot{R} = -c_{gl}k_{gl}\ln(1 + B_M) \quad \text{at } r = R, \tag{46}$$

$$w = 0, \qquad R = 1 \quad \text{at } t = 0, \tag{47}$$

where

$$f(t) = -\frac{c_2}{c_1}\operatorname{erfc}\left(\frac{1}{2\sqrt{t}}\right) + \frac{c_2}{c_1}e^{c_1 + c_1^2 t}\operatorname{erfc}\left(\frac{1 + 2c_1 t}{2\sqrt{t}}\right), \tag{48}$$

$$\begin{aligned} g(R,t) &= R\left(k_{gl}T_g - \frac{\partial \hat{v}}{\partial r}(R,t)\right) - c_1\hat{v}(R,t) \\ &= k_{gl}T_g R + c_2(1-R)e^{c_1(1-R)+c_1^2 t}\operatorname{erfc}\left(\frac{1 - R + 2c_1 t}{2\sqrt{t}}\right) - c_2\operatorname{erfc}\left(\frac{1-R}{2\sqrt{t}}\right), \end{aligned} \tag{49}$$

$$B_M = \frac{M_f}{M_g}\left(P_g \exp\left[\frac{\beta R}{w(R,t) + \hat{v}(R,t) + \gamma R} - a\right] - 1\right)^{-1}. \tag{50}$$

The next step is to immobilize the boundary by setting

$$\xi = \frac{r}{R(t)}, \qquad w(r,t) = F(\xi, t). \tag{51}$$

Then, the problem transforms into

$$\frac{\partial^2 F}{\partial \xi^2} = R^2\frac{\partial F}{\partial t} - R\dot{R}\,\xi\frac{\partial F}{\partial \xi}, \quad 0 < \xi < 1,\ 0 < t < t_e, \tag{52}$$

$$F = f(t) \quad \text{at } \xi = 0, \tag{53}$$

$$\frac{\partial F}{\partial \xi} + c_1 F = g(R,t) + R^2\dot{R} \quad \text{at } \xi = 1, \tag{54}$$

$$R\dot{R} = -c_{gl}k_{gl}\ln(1 + B_M) \quad \text{at } \xi = 1, \tag{55}$$

$$F = 0, \qquad R = 1 \quad \text{at } t = 0. \tag{56}$$

Nevertheless, this formulation is not optimal since $R \sim (t_e - t)^{1/2}$ in the limit $t \to t_e^-$, so that $\dot{R}$ is infinite in this limit. We therefore set $Z := R^2$, so that $\dot{Z} = 2R\dot{R}$; clearly, $\dot{Z}$ is finite as $t \to t_e^-$. In addition, and as demonstrated in [23], it is useful to change the time variable to $\tau := t/t_e$. Then, Eqs. (52)–(56) become

$$t_e\frac{\partial^2 F}{\partial \xi^2} = Z\frac{\partial F}{\partial \tau} - \frac{1}{2}\dot{Z}\,\xi\frac{\partial F}{\partial \xi}, \quad 0 < \xi < 1,\ 0 < \tau < 1, \tag{57}$$

$$F = f(\tau) \quad \text{at } \xi = 0, \tag{58}$$

$$t_e\left(\frac{\partial F}{\partial \xi} + c_1 F\right) = t_e g(Z,\tau) + \frac{1}{2}\sqrt{Z}\dot{Z} \quad \text{at } \xi = 1, \tag{59}$$

$$\frac{1}{2}\dot{Z} = -t_e c_{gl} k_{gl} \ln(1 + B_M) \quad \text{at } \xi = 1, \tag{60}$$

$$F = 0, \qquad Z = 1 \quad \text{at } \tau = 0, \tag{61}$$

where now the dot denotes differentiation with respect to τ, and

$$f(\tau) = -\frac{c_2}{c_1}\operatorname{erfc}\left(\frac{1}{2\sqrt{t_e\tau}}\right) + \frac{c_2}{c_1}e^{c_1 + c_1^2 t_e \tau}\operatorname{erfc}\left(\frac{1 + 2c_1 t_e \tau}{2\sqrt{t_e\tau}}\right), \tag{62}$$

$$g(Z,\tau) = k_{gl}T_g\sqrt{Z} + c_2(1-\sqrt{Z})e^{c_1(1-\sqrt{Z}) + c_1^2 t_e\tau}\operatorname{erfc}\left(\frac{1-\sqrt{Z} + 2c_1 t_e\tau}{2\sqrt{t_e\tau}}\right) - c_2\operatorname{erfc}\left(\frac{1-\sqrt{Z}}{2\sqrt{t_e\tau}}\right). \tag{63}$$

Note that B_M is again given by (50) but with $w(R,t)$ replaced by $F(1,t)$ and R replaced by $\sqrt{Z}$.

The advantage of performing numerical integration in τ, rather than in t, is that it provides a systematic way to iterate for and determine t_e. Integration is carried out on a fixed mesh for $0 \le \tau \le 1$, which then enables us to determine the scheme convergence index, $\bar{p}_\phi$, for each variable ϕ that is of interest; for more details on the definition of the convergence index, see Section 4 and [21,25]. However, because the extent of the region of interest is shrinking as $\tau \to 1$, a further elaboration, which was not required in [23], is necessary: although there is no unique way to do this, we employ the transformation

$$\tau = 1 - \exp\left(-\hat{\tau}\right), \quad \text{where } 0 \le \hat{\tau} < \infty, \tag{64}$$

which introduces a stretching in the variable τ as $\tau \to 1$ and serves in better capturing the behaviour of Z as $t \to t_e$. In the interests of brevity, we have not included here the transformed version of Eqs. (57)–(61). In practice, it is of course necessary to terminate the computations at some finite value of $\hat{\tau}$, which we denote as $\hat{\tau}_\infty$; we have taken $\hat{\tau}_\infty$ so that $1-\tau = \mathcal{O}(10^{-9})$, implying that $\hat{\tau}_\infty = 20$.

For this formulation, a strategy is necessary that is able to determine Z and t_e. Since the time domain is now fixed, we can choose $N+1$ points whereby $\hat{\tau}^n = n\Delta\hat{\tau}$, for $n = 0, 1, \ldots, N$, and with $\Delta\hat{\tau} = \hat{\tau}_\infty/N$. We use a nonlinear solver to determine Z^n, for $n = 1, 2, \ldots, N$, along with t_e, leading to $N+1$ unknowns. Either of the boundary conditions, (59) or (60), can be used to give N nonlinear equations, and then the final equation is simply $Z^N = 0$. In practice, we make an initial guess for t_e and solve for F and Z up to $\hat{\tau} = \hat{\tau}_\infty$; in general, we will obtain $Z^N \ne 0$, but the discrepancy can be used as a basis for making a new guess for t_e, and re-solving. This procedure is then repeated until the desired tolerance is reached. Denoting by $Z^N_{(m)}$ the value of Z^N obtained on the mth iteration, the convergence criterion used is

$$\left|Z^N_{(m)}\right| < \epsilon.$$

The value of ϵ used turns out to be of particular importance for the numerical solution in the limit as $t \to t_e^-$; we examine this in more detail in Section 4.3.

Lastly, we note one of the *disadvantages* of this new formulation. The variable t_e now appears explicitly in the governing equations, yet its value is not known *a priori*; consequently, we cannot find the solution at any value of r and t before we find t_e. On the other hand, the original formulation in [1] *did* enable us to find the solution at any value of r and t finding t_e, but did not give us a strategy for finding t_e; however, in what follows, we will be able to compare the results of the two formulations.

4. Results

In summary, we present results from four different formulations:

(I) Eqs. (21)–(24);
(II) Eqs. (38)–(41);
(III) Eqs. (52)–(56);
(IV) Eqs. (57)–(61) with transformation (64).

In fact, results from all of these prove necessary to provide a complete picture of the solution to the problem. As in [1], we use the Keller box scheme; the reader is referred to the earlier paper, along with [20], for full details of the numerical discretization. Here, we summarize the main ideas by applying the box scheme to (52)–(56), as an example. The PDE (52) must be written as a first-order system by setting $G = \partial F/\partial\xi$. For a general dependent variable ϕ and general independent

time- and space-like variables, X and Y respectively, we define the following finite difference operators:

$$\mu_X \phi_{i+\frac{1}{2}}^{n+\frac{1}{2}} = \frac{\phi_{i+\frac{1}{2}}^{n+1} + \phi_{i+\frac{1}{2}}^{n}}{2}, \qquad \delta_X \phi_{i+\frac{1}{2}}^{n+\frac{1}{2}} = \frac{\phi_{i+\frac{1}{2}}^{n+1} - \phi_{i+\frac{1}{2}}^{n}}{\Delta X}, \tag{65}$$

$$\mu_Y \phi_{i+\frac{1}{2}}^{n+\frac{1}{2}} = \frac{\phi_{i+1}^{n+\frac{1}{2}} + \phi_{i}^{n+\frac{1}{2}}}{2}, \qquad \delta_Y \phi_{i+\frac{1}{2}}^{n+\frac{1}{2}} = \frac{\phi_{i+1}^{n+\frac{1}{2}} - \phi_{i}^{n+\frac{1}{2}}}{\Delta Y}. \tag{66}$$

With $X = t,\ Y = \xi$, the box scheme applied to (52) therefore gives, for $n = 0, 1, 2, \ldots,$

$$\mu_t \delta_\xi F_{i+\frac{1}{2}}^{n+\frac{1}{2}} = \mu_t \mu_\xi G_{i+\frac{1}{2}}^{n+\frac{1}{2}}, \tag{67}$$

$$\mu_t \delta_\xi G_{i+\frac{1}{2}}^{n+\frac{1}{2}} = \left(\mu_t R^{n+\frac{1}{2}}\right)^2 \mu_\xi \delta_t F_{i+\frac{1}{2}}^{n+\frac{1}{2}} - \left(\mu_\tau R^{n+\frac{1}{2}}\right)\left(\delta_t R^{n+\frac{1}{2}}\right)\left(\mu_\xi \xi_{i+\frac{1}{2}}\right)\mu_t \mu_\xi G_{i+\frac{1}{2}}^{n+\frac{1}{2}}, \tag{68}$$

which holds for $i = 1, \ldots, I-1$. Boundary conditions (53)–(55) become

$$\mu_t F_0^{n+\frac{1}{2}} = \mu_t f^{n+\frac{1}{2}}, \tag{69}$$

$$\mu_t G_I^{n+\frac{1}{2}} + c_1 \mu_t F_I^{n+\frac{1}{2}} = \mu_t g^{n+\frac{1}{2}} + \left(\mu_t R^{n+\frac{1}{2}}\right)^2 \left(\delta_t R^{n+\frac{1}{2}}\right), \tag{70}$$

$$\left(\mu_t R^{n+\frac{1}{2}}\right)\left(\delta_t R^{n+\frac{1}{2}}\right) = -c_{gl} k_{gl} \ln\left(1 + B_M^{n+\frac{1}{2}}\right), \tag{71}$$

where

$$B_M^{n+\frac{1}{2}} = \frac{M_g}{M_f}\left(P_g \exp\left[\frac{\beta \mu_t R^{n+\frac{1}{2}}}{\mu_t F_I^{n+\frac{1}{2}} + \mu_t \hat{v}^{n+\frac{1}{2}} + \gamma \mu_t R^{n+\frac{1}{2}}} - a\right] - 1\right)^{-1}. \tag{72}$$

Finally, the initial conditions are simply $F_i^0 = 0$ and $R^0 = 1$.

It should be noted that, since (68) involves R^{n+1}, it is necessary to solve a nonlinear equation at each timestep. This is achieved by iterating on R, using the value at level n as a starting guess. More details on this can be found in [1,20].

We also wish to determine the order of accuracy of our numerical scheme. Consider a sequence ΔY_j where

$$\Delta Y_j = 2^{-j} \Delta Y_0, \quad j = 1, 2, \ldots,$$

and the space coordinates of meshes associated with this sequence are denoted by

$$Y_{i,j} = i \Delta Y_j, \quad i = 0, 1, \ldots, I_j,\ j = 0, 1, 2, \ldots,$$

where

$$I_j = 2^j I_0, \quad j = 1, 2, \ldots.$$

As discussed in [25], for a general numerical solution $U_{2^j i}^n$ and corresponding exact solution $\mathcal{U}(Y_{i,j}, X^n)$ to the heat conduction equation at the nth time-like step, X^n, the error and corresponding order of convergence, $E_{U,j}^n$ and $p_{U,j}$ respectively, are given by

$$E_{U,j}^n = \left(\Delta Y_j \sum_{i=0}^{I_0} \left(\mathcal{U}(Y_{i,0}, X^n) - U_{2^j i}^n\right)^2\right)^{1/2}, \qquad p_{U,j} = \frac{\ln(E_{U,j}^n / E_{U,j+1}^n)}{\ln 2}, \tag{73}$$

for $j = 0,\ 1,\ 2, \ldots$. In order to be able to make use of (73), it is necessary that an exact solution is known; thus, $p_{U,j}$ constitutes the accuracy of the solution. However, when an exact solution is not known, the best one can do is to determine the accuracy of the numerical scheme [20]. To do this, instead of $E_{U,j}^n$ in (73), we define, for $j = 1,\ 2, \ldots$

$$\bar{E}_{U,j}^n = \left(\sum_{i=0}^{I_0} \left(U_{2^j i}^n - U_{2^{j-1} i}^n\right)^2\right)^{1/2}, \qquad \bar{p}_{U,j} = \ln(\bar{E}_{U,j}^n / \bar{E}_{U,j+1}^n) / \ln 2; \tag{74}$$

in cases where an exact solution was known, Mitchell and Vynnycky [20] showed that $p_U = \bar{p}_U$, where

$$p_U = \lim_{j \to \infty} p_{U,j}, \qquad \bar{p}_U = \lim_{j \to \infty} \bar{p}_{U,j}.$$

Table 2
Comparison of the order of accuracy of the numerical solution for formulation I, for v and v_r at fixed $t = 0.1$ and $\nu(= \Delta t/\Delta r) = 0.1$.

Δr (k)	$\bar{p}_v$	$\bar{p}_{v_r}$
1/40 ($k = 2$)	1.95625	1.79252
1/80 ($k = 3$)	1.57648	2.31532
1/160 ($k = 4$)	1.11330	7.36133
1/320 ($k = 5$)	0.99962	2.35167

Table 3
Comparison of the order of accuracy of the numerical solution for formulation II, for w and w_r at fixed $t = 0.1$ and $\nu(= \Delta t/\Delta r) = 0.1$.

Δr (k)	$\bar{p}_w$	$\bar{p}_{w_r}$
1/40 ($k = 2$)	2.03689	2.02618
1/80 ($k = 3$)	2.00919	2.00661
1/160 ($k = 4$)	2.00229	2.00166
1/320 ($k = 5$)	2.00057	2.00041

However, they applied this only to the temperature, i.e. $\mathcal{U}$; here, in contrast, we will apply it also to the spatial derivative of the temperature, $\partial\mathcal{U}/\partial Y$, and the location of the moving boundary which, for this general discussion, we denote by $\mathcal{S}(X)$. Thus, writing $\mathcal{V} = \partial\mathcal{U}/\partial Y$, we define, analogously to (73) and (74), for $j = 1, 2, \ldots$

$$E^n_{V,j} = \left(\Delta Y_j \sum_{i=0}^{I_0} \left(\mathcal{V}(Y_{i,0}, t^n) - V^n_{2^j i}\right)^2\right)^{1/2}, \qquad p_{V,j} = \frac{\ln(E^n_{V,j}/E^n_{V,j+1})}{\ln 2}, \tag{75}$$

$$\bar{E}^n_{V,j} = \left(\sum_{i=0}^{I_0} \left(V^n_{2^j i} - V^n_{2^{j-1} i}\right)^2\right)^{1/2}, \qquad \bar{p}_{V,j} = \ln(\bar{E}^n_{V,j}/\bar{E}^n_{V,j+1})/\ln 2, \tag{76}$$

$$E^n_{\mathcal{S},j} = \left|\mathcal{S}(X^n) - \mathcal{S}^n_j\right|, \qquad p_{\mathcal{S},j} = \ln(E^n_{\mathcal{S},j}/E^n_{\mathcal{S},j+1})/\ln 2, \tag{77}$$

$$\bar{E}^n_{\mathcal{S},j} = \left|\mathcal{S}^n_j - \mathcal{S}^n_{j-1}\right|, \qquad \bar{p}_{\mathcal{S},j} = \ln(\bar{E}^n_{\mathcal{S},j}/\bar{E}^n_{\mathcal{S},j+1})/\ln 2, \tag{78}$$

where $(V^n_{2^j i}, \mathcal{S}^n_j)$ and $(\mathcal{V}(Y_{i,j}, X^n), \mathcal{S}(X^n))$ denote, respectively, the numerical and exact solutions to the heat conduction equation at the nth time step; in addition, we define

$$\bar{p}_V = \lim_{j\to\infty} \bar{p}_{V,j}, \qquad \bar{p}_{\mathcal{S}} = \lim_{j\to\infty} \bar{p}_{\mathcal{S},j}.$$

The $\bar{p}$ values given in (74), (76) and (78) are used in the discussion below.

4.1. Small-time problem

The convergence indices for the box scheme applied to formulations I and II are given in Tables 2 and 3, respectively; in the tables, the parameter k indicates the degree of mesh refinement. In Table 2, there is no discernible pattern as a finer mesh is used; in Table 3, $\bar{p}_v$ and $\bar{p}_{v_r}$ both tend to 2 as the mesh is refined, indicating second-order accuracy for the dependent variable and its spatial derivative, as expected [21–23]. Once again, this emphasizes the need for an analytical pre-treatment of the governing equations in order to find a formulation that leads to a numerical solution that is second-order accurate in both time and space variables.

4.2. Full problem

Table 4 shows the convergence indices for formulation IV; these indicate second-order accuracy for F, G, Z and t_e. Moreover, Table 5 shows the value of t_e obtained as the mesh is refined. Fig. 3 compares R as a function of t, as obtained numerically with formulations III and IV; this illustrates how formulation IV is better able to resolve the behaviour of R as $R \to 0$. For brevity, we have not included a convergence index table for formulation III; as in [1], F, G and R were all obtained with second-order accuracy.

4.3. $t \to t_e$

In the remaining figures, we examine the performance of formulation IV in the limit as $t \to t_e$; unless otherwise stated, we take $\epsilon = 10^{-8}$. Setting $\zeta = 1 - \tau$, Fig. 4 shows Z as a function of ζ for $k = 2, 3, 4$; comparison is made with the analytical expression derived in [1],

$$Z = \lambda^2 t_e \zeta, \tag{79}$$

Table 4
Comparison of the order of accuracy of the numerical solution for formulation IV, for F, G ($= F_\xi$) and Z at fixed $\hat{\tau} = 2$ and $\nu(= \Delta\hat{\tau}/\Delta\xi) = 0.8$.

$\Delta\xi$ (k)	$\bar{p}_F$	$\bar{p}_G$	$\bar{p}_Z$	$\bar{p}_{t_e}$
1/40 ($k = 2$)	1.99643	2.05670	2.00543	2.00153
1/80 ($k = 3$)	2.00024	1.98781	2.00172	2.00122
1/160 ($k = 4$)	2.00008	2.00086	2.00156	2.00098

Table 5
t_e for $k = 0, 1, \ldots, 4$, as obtained with formulation IV.

k	0	1	2	3	4
t_e	0.591048	0.591233	0.591278	0.591290	0.591293

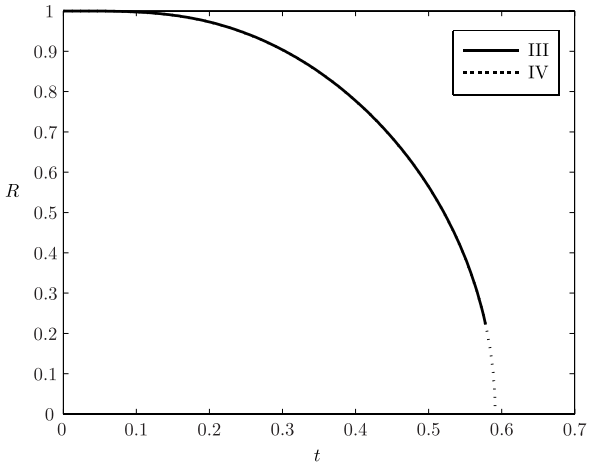

Fig. 3. R vs. t for formulations III and IV.

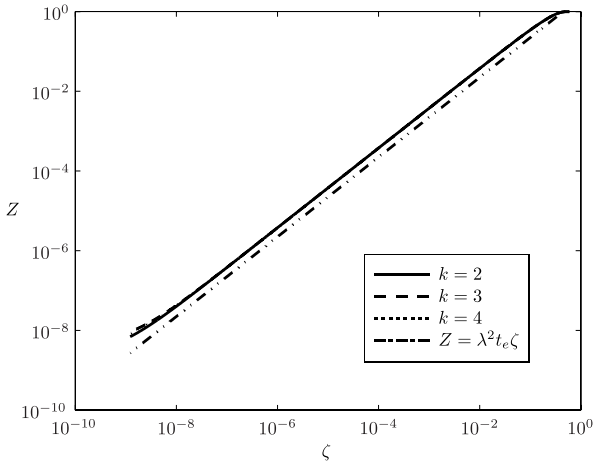

Fig. 4. Z vs. ζ for formulation IV ($k = 2, 3, 4$) and the line $Z = \lambda^2 t_e \zeta$.

where λ is given by

$$\lambda = \sqrt{2k_{gl}\left(T_g - \chi\right)}, \tag{80}$$

and χ satisfies

$$\exp\left(\frac{T_g - \chi}{c_{gl}} - 1\right)\left(P_g \exp\left(\frac{\beta}{\chi + \gamma} - a\right) - 1\right) = \frac{M_f}{M_g}. \tag{81}$$

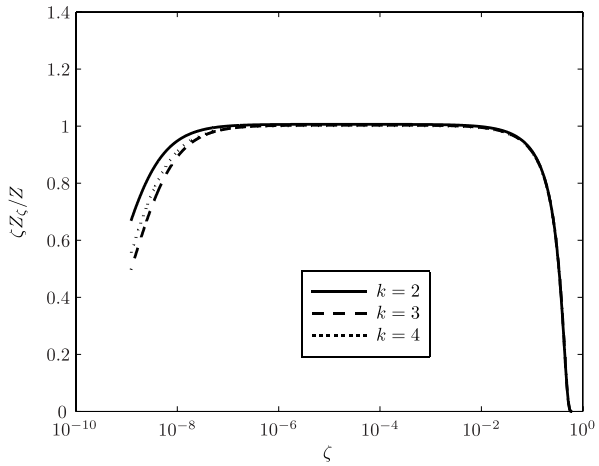

Fig. 5. $\zeta Z_\zeta / Z$ vs. ζ for formulation IV ($k = 2, 3, 4$).

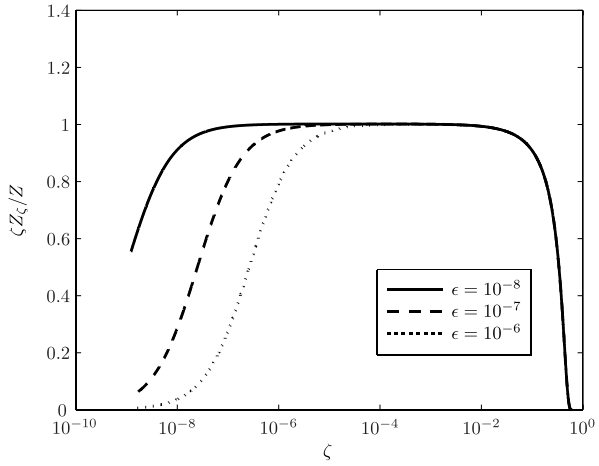

Fig. 6. $\zeta Z_\zeta / Z$ vs. ζ for formulation IV with $k = 4$ ($\epsilon = 10^{-8}, 10^{-7}, 10^{-6}$).

Note that although (79) is a closed-form expression for Z, it does rely on the constant t_e which can only be computed numerically. This notwithstanding, we find very good agreement between the numerical solution and the asymptotic estimate.

Fig. 5 which shows $\zeta Z_\zeta / Z$ as a function of ζ for $k = 2, 3, 4$, again for formulation IV. The analysis indicates that

$$\lim_{\zeta \to 0} \zeta Z_\zeta / Z = 1,$$

and this is indeed what is observed numerically for ζ as low as 10^{-6}. Thereafter, however, we see an undesired dip in the curves, and this is investigated further in Fig. 6, which shows $\zeta Z_\zeta / Z$ as a function of ζ for $k = 4$, but for three different values of ϵ, and again for formulation IV. From this figure, it is evident that the value of ϵ chosen has an effect on the value of ζ at which the dip begins to appear in $\zeta Z_\zeta / Z$. The suggestion is that, by decreasing ϵ, it should be possible to shift the onset of numerical oscillations to smaller values of ζ, although at greater computational expense.

5. Conclusions

In this contribution, we have developed a numerical algorithm, based around the Keller box finite-difference scheme and the boundary immobilization method, for solving a Stefan problem that has a finite extinction time, i.e. when the phase that was initially present becomes depleted. Although we have considered analysis for the particular problem of droplet evaporation [1], the method is general enough to be applicable to other problems of practical interest [9–18].

Acknowledgement

The second author acknowledges the support of the Mathematics Applications Consortium for Science and Industry (www.macsi.ul.ie) funded by the Science Foundation Ireland grant 12/IA/1683.

References

[1] S.L. Mitchell, M. Vynnycky, I.G. Gusev, S.S. Sazhin, An accurate numerical solution for the transient heating of an evaporating droplet, Appl. Math. Comput. 217 (2011) 9219–9233.
[2] S.S. Sazhin, P.A. Krutitskii, I.G. Gusev, M.R. Heikal, Transient heating of an evaporating droplet, Int. J. Heat Mass Transfer 53 (2010) 2826–2836.
[3] R.I. Pedroso, G.A. Domoto, Perturbation solutions for spherical solidification of saturated liquids, J. Heat Transfer 95 (1973) 42–46.
[4] D.S. Riley, F.T. Smith, G. Poots, The inward solidification of spheres and circular cylinders, Int. J. Heat Mass Transfer 17 (1974) 1507–1516.
[5] K. Stewartson, R.T. Waechter, On Stefan's problem for spheres, Proc. R. Soc. A 348 (1976) 415–426.
[6] A.M. Soward, A unified approach to Stefan's problem for spheres, Proc. R. Soc. A 373 (1980) 131–147.
[7] M.A. Herrero, J.J.L. Velazquez, On the melting of ice balls, SIAM J. Math. Anal. 28 (1997) 1–32.
[8] S.W. McCue, B. Wu, J.M. Hill, Classical two-phase Stefan problem for spheres, Proc. R. Soc. A 464 (2008) 2055–2076.
[9] M. Vynnycky, A mathematical model for air-gap formation in vertical continuous casting: the effect of superheat, Trans. Indian Inst. Met. 62 (2009) 495–498.
[10] M. Vynnycky, An asymptotic model for the formation and evolution of air gaps in vertical continuous casting, Proc. R. Soc. Lond. Ser. A Math. Phys. Eng. Sci. 465 (2009) 1617–1644.
[11] M. Vynnycky, Air gaps in vertical continuous casting in round moulds, J. Engrg. Math. 68 (2010) 129–152.
[12] M. Vynnycky, On the role of radiative heat transfer in air gaps in vertical continuous casting, Appl. Math. Model. 37 (2013) 2178–2188.
[13] M. Vynnycky, On the onset of air-gap formation in vertical continuous casting with superheat, Int. J. Mech. Sci. 73 (2013) 69–76.
[14] J. Crank, R.S. Gupta, A moving boundary problem arising from the diffusion of oxygen in absorbing tissue, J. Inst. Math. Appl. 10 (1972) 19–33.
[15] A. Boureghda, Numerical solution of the oxygen diffusion in absorbing tissue with a moving boundary, Comm. Numer. Methods Engrg. 22 (2006) 933–942.
[16] A. Boureghda, Numerical solution of the oxygen diffusion problem in cylindrically shaped sections of tissue, Int. J. Numer. Methods Fluids 56 (2008) 1945–1960.
[17] V. Gülkaç, Comparative study between two numerical methods for oxygen diffusion problem, Comm. Numer. Methods Engrg. 25 (2009) 855–863.
[18] S.W. McCue, M. Hsieh, T.J. Moroney, M.I. Nelson, Asymptotic and numerical results for a model of solvent-dependent drug diffusion through polymeric spheres, SIAM J. Appl. Math. 71 (2011) 2287–2311.
[19] S. Tabakova, F. Feuillebois, S. Radev, Freezing of a supercooled spherical droplet with mixed boundary conditions, Proc. R. Soc. A 466 (2010) 1117–1134.
[20] S.L. Mitchell, M. Vynnycky, Finite-difference methods with increased accuracy and correct initialization for one-dimensional Stefan problems, Appl. Math. Comput. 215 (2009) 1609–1621.
[21] S.L. Mitchell, M. Vynnycky, An accurate finite-difference method for ablation-type Stefan problems, J. Comput. Appl. Math. 236 (2012) 4181–4192.
[22] M. Vynnycky, S.L. Mitchell, On the accuracy of a finite-difference method for parabolic PDEs with discontinuous boundary conditions, Numer. Heat Transfer Part B 64 (2013) 275–292.
[23] S.L. Mitchell, M. Vynnycky, On the numerical solution of two-phase Stefan problems with heat-flux boundary conditions, J. Comput. Appl. Math. 264 (2014) 49–64.
[24] S.S. Sazhin, Advanced models of fuel droplet heating and evaporation, Prog. Energy Combust. Sci. 32 (2) (2006) 162–214.
[25] J.C. Strikwerda, Finite Difference Schemes and Partial Differential Equations, second ed., Society for Industrial Mathematics, 2004.